Dispersion-Tuned Mode-Locked Laser for Swept Source OCT at 850 nm Using a cFBG and the Pulse Modulation Technique

Rene Riha, Alejandro Martinez Jimenez, Gopika Venugopal, Marie Klufts, Robert Huber, and Adrian Podoleanu, *Senior Member, IEEE*

***Abstract*—In this paper, the feasibility of employing a fast intensity modulator and a chirped fibre Bragg grating to build a dispersion-tuned mode-locked swept laser (DTML-SS) for OCT at 850 nm is evaluated. Stable mode-locking is achieved by applying 50 ps pulses at 1 GHz to the modulator, obtaining 35 nm tuning range at 10 KHz sweep rate and 1 mm axial range.**

***Index Terms*—cFBG, intensity modulator, dispersion tuning, OCT.**

I. Introduction

AN OPTICAL coherence tomography (OCT) method that examines the optical spectrum at the output of an interferometer is the swept source OCT (SS-OCT). Most of the research on SS-OCT is spurred by the recent developments in the field of swept sources. The axial range, the axial resolution, and the measurement speed of SS-OCT are all dependent on the characteristics of the swept source.

Several concepts of wavelengh tuning have been reported, such as a galvo filter-based [1], micro-electromechanical system vertical cavity surface-emitting laser (MEMS-VCSEL) [2], Fourier domain mode-locked laser (FDML) technology [3], Vernier tuning [4], time-stretch technology [5], or stretched-pulse mode-locking (SPML) [6].

Advancements in the swept source technology focus on two main aspects: (i) increasing the sweep rates, and (ii) extending the operational wavelength towards shorter wavelengths. Faster sweep rates, ranging from a few kHz to tens of MHz, are essential for flying spot OCT, which involves deflecting an optical beam over a sample [7]. Extending the operational wavelength to shorter regions is particularly important for full field swept source (FFSS)-OCT technology which utilises CMOS 2D cameras [7], [8]. Given the spectral sensitivity of CMOS, the swept source (SS) should operate at wavelengths shorter than 850 nm. Currently, the only commercially available swept sources for FFSS-OCT are acousto-optic tunable filter (AOTF) based, produced by Superlum Ireland [9]. However, the principle of the AOTF deflection limits the wavelength tuning to a 2 kHz sweep rate. Important for broadening OCT applications is also the miniaturisation. In this respect, an AOTF based swept source is a free space device relying on a diffraction grating for the wavelength tuning, which poses limitations to the miniaturisation.

This paper presents the concept of a tunable laser for FFSS-OCT, based on all in fibre components, akinetic, and compatible with miniaturisation. This implements dispersion-tuned mode-locking (DTML) [10]. A DTML laser consists of three main elements: a gain medium, a modulation (mode-locking) element, and a dispersive element. In general, for good stability and coherence properties, the temporal modulation window should be narrow ($\lesssim 100$ ps) and dispersion high ($\gtrsim 10$ ps/nm) [10].

First DTML-SS reports employed long pieces (~ 100 m) of fibers as a dispersive element, operating at different wavelengths [11], 850 nm, 1300 nm, or 1550 nm. Utilising long length dispersive cavities, sweep rates of only a few kHz were obtained. Using a chirped fiber Bragg grating (cFBG), shorter cavity lengths are achievable that allowed larger sweep rates of tens of kHz at 1300 nm [12] and at 1550 nm [13]. As shown in [14], anomalous dispersion creates a narrower linewidth than normal dispersion, and by utilising a cFBG, anomalous dispersion is ensured even for wavelengths where fibre exhibits normal dispersion.

In the references listed above, a semiconductor optical amplifier (SOA) was employed for both gain and mode-locking. Such a solution has several drawbacks. First, not only that the gain is modulated, but other parameters such as the gain spectral bandwidth. Also, the RF bandwidth of the SOA circuitry is limited up to ~ 500 MHz. The practice in DTML shows that sub-nanosecond pulse modulation instead of sinusoidal modulation improves the tuning range and reduces the amplified spontaneous emission (ASE) [10], [15]. This is achievable by employing a high speed intensity modulator instead of modulating the SOA, solution that also enables a more stable operation

Manuscript received 9 June 2024; accepted 18 June 2024. Date of publication 21 June 2024; date of current version 1 July 2024. The work of Adrian Podoleanu was supported in part by UCL Institute of Ophthalmology and Moorfields Eye Hospital, in part by NIHRBRC4-05-RB413-302, in part by MRC Impact Accelerator Account under Project 18557, in part by i4i Call 21 under Grant NIHR202879, and in part by the BBSRC under Grant BB/S0166431. This work was supported by EC for NETLAS ITN under Grant Agreement Number 860807. *(Corresponding author: Rene Riha.)*

Rene Riha, Alejandro Martinez Jimenez, Gopika Venugopal, and Adrian Podoleanu are with the Applied Optics Group, School of Physical Sciences, University of Kent, CT2 7NH Canterbury, U.K. (e-mail: rr406@kent.ac.uk).

Marie Klufts and Robert Huber are with the Institut für Biomedizinische Optik, Universität zu Lübeck, 23562 Lübeck, Germany.

Digital Object Identifier 10.1109/JPHOT.2024.3417829

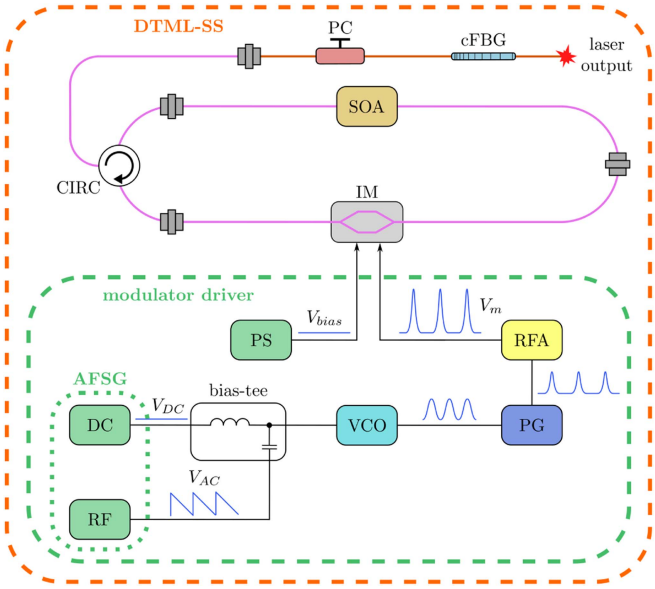

Fig. 1. DTML laser. SOA: semiconductor optical amplifier, IM: intensity modulator, CIRC: optical circulator, PC: polarisation controller, cFBG: chirped fiber Bragg grating, AFSG: arbitrary function signal generator, VCO: voltage-controlled oscillator, PG: pulse generator, RFA: RF amplifier, PS: power supply.

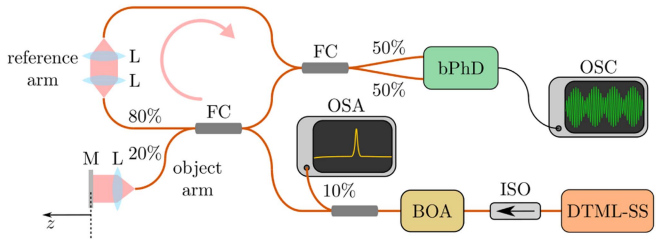

Fig. 2. SS-OCT setup used for characterisation of the DTML in Fig. 1. The re-circulation of the reference wave is depicted with an arrow. DTML: dispersion tuned mode-locked laser, ISO: isolator, BOA: booster optical amplifier, OSA: optical spectrum analyser, FC: fiber coupler, L: launcher lens system, M: mirror, bPhD: balanced photodetector block, OSC: oscilloscope.

for the active medium as was demonstrated at 1060 nm [10] and at 1550 nm [15].

In this letter, we demonstrate that the technologies of fast and short pulse modulation together with that of cFBGs have matured enough to be applied to DTML at shorter wavelengths such as 850 nm.

II. Methods

The DTML-SS studied in this report is depicted in Fig. 1. The swept source is constructed from three key components: a semiconductor optical amplifier, SOA (Superlum SOA-372, optical gain bandwidth 40 nm), an intensity modulator, IM (Exail NIR-MX800-LN-20, RF bandwidth 20 GHz), and a chirped fiber Bragg grating, cFBG (Teraxion PSR-840-72(+D16.77-0.035)-0S1-0R, reflection bandwidth 72 nm, reflectivity 90%, dispersion 17 ps/nm). The SOA acts as the gain medium, the IM as the mode-locking element and the cFBG as the dispersive element. The operational wavelength and bandwidth of the swept source are mainly determined by the employed SOA. The light is directed to the cFBG through an optical circulator, CIRC (OZ Optics FOC-12P-111-6/125-PPP-1060-50-3A3A3A-1-1-WB, optical bandwidth 100 nm), which serves also as an optical isolator in the cavity. The light is then coupled out in transmission through the cFBG. The cFBG employs single mode fiber via a polarisation controller (PC). The rest of the cavity consists of polarisation maintaining fiber. The total cavity round trip length is evaluated as 13.6 m (free spectral range of 15.1 MHz) and effective dispersion is estimated as 14.6 ps/nm using the technique described in [16].

A schematic diagram of the intensity modulator driver is detailed in Fig. 1 as well (inside the green dashed rectangle). A voltage-controlled oscillator, VCO (Mini-Circuits ZX95-1240-S+, 1-2 GHz), is driven with DC, V_{DC}, and AC, V_{AC}, voltage signals from an arbitrary function signal generator, AFSG (Agilent Technologies 81160 A). Due to the maximum output voltage limitation of $V_{DC} + V_{AC}$ delivered by the AFSG, an in-house bias-tee is employed to separate the control of V_{DC} and V_{AC}. The VCO output signal is directed to a pulse generator, PG (AlnairLabs EPG-210M-0050-S-P-N-N), which generates a short pulse of width 50 ps per each period of the input signal. This means that the pulses repetition frequency f_m is that of the instantaneous input sinusoidal signal provided by the VCO. The pulses are then amplified through a pair of cascaded RF amplifiers, RFA (Mini-Circuits ZVA-01243+, 1-22 GHz, 22 dBm, and Xmicrowave XM-A3E6-0804C-01, DC-20 GHz, 25 dBm), and applied to the IM. Finally, the bias of the IM is controlled separately by DC voltage from a regulated power supply, PS.

The signal out of the cFBG is amplified through another semiconductor optical amplifier (same model as the gain medium inside the cavity, operating as a booster), BOA, and directed to an interferometer whose scheme is depicted in Fig. 2. The optical spectrum of the BOA is displayed on an optical spectrum analyser, OSA (Agilent Technologies 86145B). The interferometer consists of two couplers in an array that recirculates the reference wave to avoid light being directed back into the optical source, terminated with a balanced photodetector block, bPhD (New Focus 1607, 40 kHz to 650 MHz). The output interferometer signals are then observed on an oscilloscope, OSC (Teledyne Lecroy WaveRunner 104MXi-A). The photodetected interferometer signal is then acquired and displayed by an oscilloscope, OSC (Teledyne Lecroy WaveRunner 104MXi-A). The optical path difference, OPD, in the interferometer is adjusted by displacing the mirror M along the coordinate z from the position where the OPD $= 0$.

Wavelength tuning in DTML is obtained by sweeping the modulation frequency f_m of the signal applied to the IM. To mode-lock the cavity, the modulation frequency must match an integer number m of the fundamental resonant frequency of the cavity, $f_r(\lambda)$, which, due to the presence of the chromatic dispersion, is wavelength dependent,

$$f_m(\lambda) = m f_r(\lambda) = m \frac{c}{n(\lambda) L(\lambda)}, \tag{1}$$

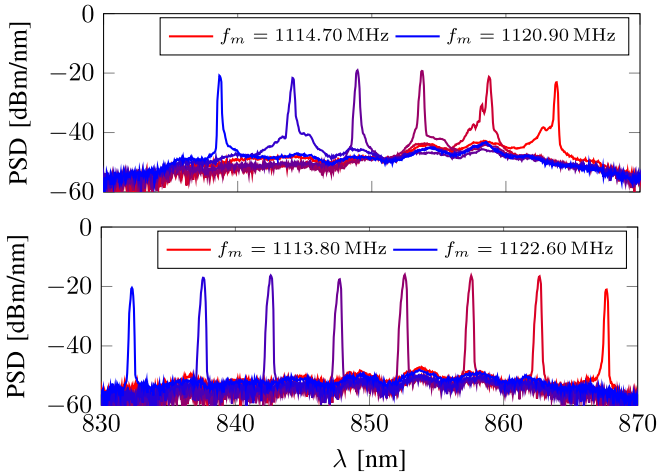

Fig. 3. Static regime spectra of the DTML laser. Top: sinusoidal modulation, bottom: pulse modulation. PSD: power spectral density.

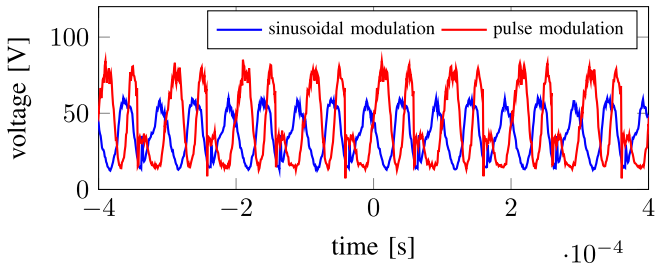

Fig. 4. Interferometer output signal using the sinusoidal and the pulse modulation for an object arm mirror distance $z = 25\ \mu$m (see Fig. 2).

where c is the speed of light in vacuum, $L(\lambda)$ is the cavity round trip length and $n(\lambda)$ is the effective group index of refraction. The chromatic dispersion in the laser cavity due to the fiber and cFBG is indicated by the wavelength λ dependence of n and L in (1). From (1), the lasing wavelength is precisely controlled by the modulation frequency f_m applied to the IM. The modulation frequency of the signal generated at the VCO's output is repeatedly swept in time by applying V_{AC} signal to the VCO's input (see Fig. 1). The VCO's central modulation frequency is determined by V_{DC} and its frequency is tuned from 1113.80 MHz to 1122.60 MHz 1122.60 MHz, as shown in Fig. 3 bottom graph. The relationship between the variation in the lasing wavelength $\Delta\lambda$ and the change in the modulation frequency Δf_m is then given by [17]

$$\Delta\lambda = -S\Delta f_m = -\frac{1}{\mathrm{TDD}_{eff} f_r f_m}\Delta f_m, \tag{2}$$

where TDD_{eff} is the effective time delay dispersion in the cavity. The proportional constant S in (2) is the so-called wavelength tuning sensitivity, which generally depends on dispersion in the cavity, cavity length and modulation frequency. An achievable tuning range is primarily determined by two factors: the gain medium optical bandwidth and the lasing at adjacent harmonic modulation frequencies $f_m(\lambda)$ and $f_m(\lambda) - f_r(\lambda)$ or $f_m(\lambda)$ and $f_m(\lambda) + f_r(\lambda)$. By substituting f_r for Δf_m in (2), the maximum wavelength tuning range $\Delta\lambda_{\max}$, conditioned by the need to avoid the lasing at adjacent harmonic modulation frequencies, can be estimated as

$$\Delta\lambda_{\max} \approx \frac{1}{|\mathrm{TDD}_{eff}| f_m}. \tag{3}$$

Given that $\mathrm{TDD}_{eff} \doteq 14.6$ ps/nm and $f_m \approx 1.1$ GHz in the study, the maximum theoretically achievable tuning range for these parameters is $\Delta\lambda_{\max} \doteq 62$ nm. However this estimation does not include the bandwidth limitation of the SOA and of the other elements in the cavity. The reason for selecting a relatively higher modulation frequency exceeding 1 GHz is to reduce the tuning sensitivity S in (2), enhancing the definition of the lasing wavelength and reduing tolerance to the instabilities and jitter in the modulation frequency f_m [17].

In DTML lasers, coherence is in general determined by the effective chromatic dispersion in the cavity, temporal window of the modulation, and sweep rate f_s. For a good wavelength filtering performance, the dispersion should be high ($\gtrsim 10$ ps/nm) and the modulation temporal window short ($\lesssim 100$ ps). Fig. 3 shows static (no fast sweeping) spectra obtained by sinusoidal modulation (modulation window width of $\approx 1/2f_m \doteq 500$ ps) and by pulse modulation technique (modulation window width of $\doteq 50$ ps), both at $f_m \doteq 1.1$ GHz. Fig. 3 illustrates three improvements due to the pulse modulation: (i) the detrimental ASE is reduced, (ii) spectral peaks are better defined, and (iii) tuning range is enlarged from 25 nm to 35 nm, in agreement with [15]. To document further the advantage of the pulse modulation in comparison with the sinusoidal modulation, Fig. 4 shows the interferometer output signals at the mirror M position $z = 25\ \mu$m (see Fig. 2). This measurement was done using the bPhD's monitor output in order to provide a proportional value to both the ASE power as well as to the fringes imprinted by the interference. The source was swept within 25 nm tuning range at 10 kHz. The fringe depth, defined as $(V_{\max} - V_{\min})/(V_{\max} + V_{\min})$, where V represents the voltage of the photodetected signal, was measured to be 0.62 and 0.72 for the sinusoidal modulation and for the pulse modulation, respectively.

By applying the pulse modulation in the static regime, the linewidth was measured as $\delta\lambda \doteq 0.09 - 0.11$ nm, which is also the narrowest linewidth achievable from the laser. When the wavelength is swept at high sweep rates (the dynamic regime), the sweeping operation of the laser usually causes a linewidth broadening [18]. For a minimum lasing operation, the sweeping must satisfy the so-called one round trip condition, limiting the sweep frequency at which each lasing wavelength circulates at least once in the cavity when being tuned [10], [19]

$$f_{s,single} \approx f_r \frac{\delta\lambda}{\Delta\lambda}. \tag{4}$$

For instance, substituting $f_r = 15.1$ MHz, $\delta\lambda = 0.1$ nm and $\Delta\lambda = 35$ nm (the tuning range achieved in Fig. 3 bottom graph) into (4), the sweep rate should not exceed 40 kHz to fulfil the one round trip condition. However, for good lasing properties, such as decent output power and narrow linewidth, the lasing should reach gain saturation in the cavity and condition (4) usually gives sweep rates too high to achieve that [19]. As a rule of thumb,

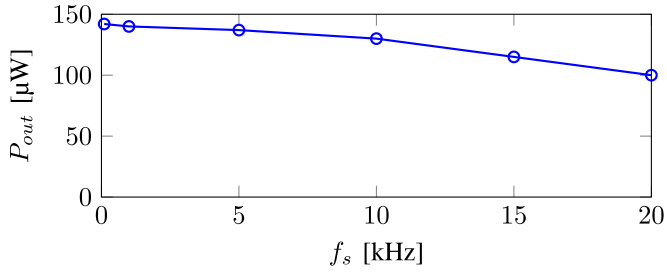

Fig. 5. Power measured at the DTML-SS output against sweep frequency f_s.

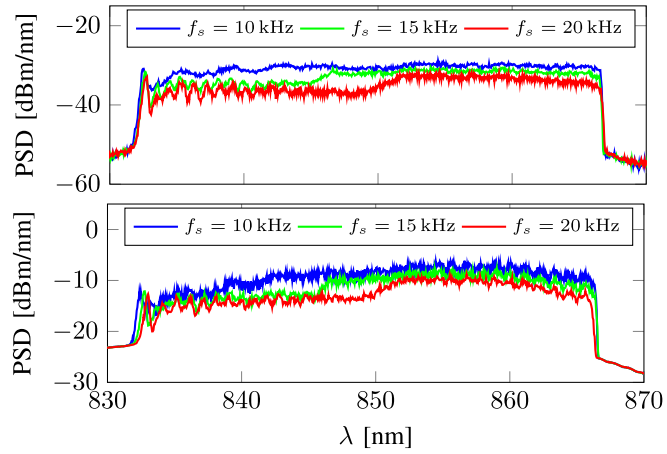

Fig. 6. Dynamic regime lasing spectra. Top: DTML-SS's output, bottom: after BOA amplification. PSD: power spectral density.

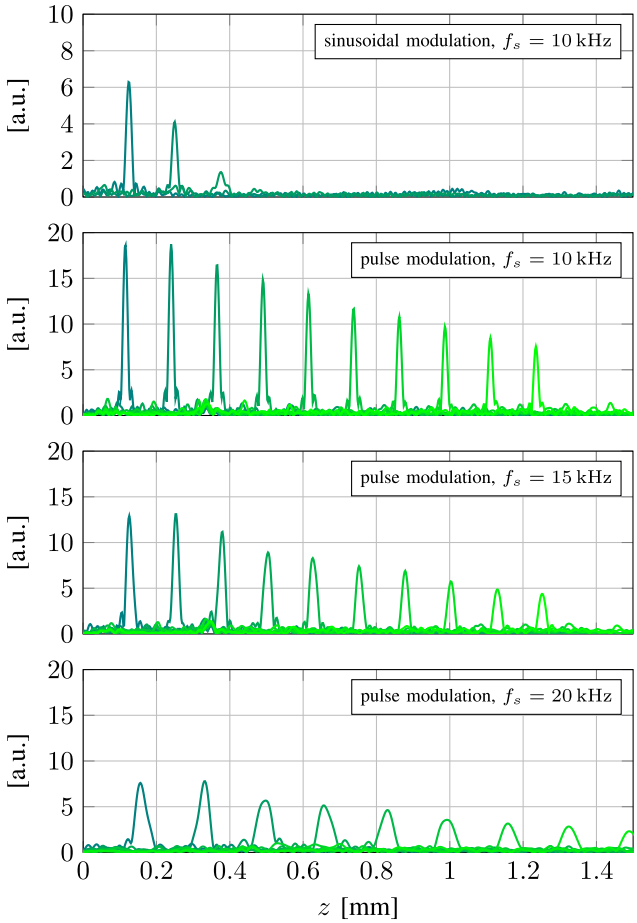

Fig. 7. A-scan roll-off measurements against distance z in Fig. 2.

gain saturation is achieved after at least three round trips in the cavity, which limits the sweep frequency according to

$$f_{s,sat} \approx f_{s,single}/3 = f_r \frac{\delta\lambda}{\Delta\lambda}/3. \quad (5)$$

Substituting the same parameters as for (4) into (5), it results that the sweep rate should not exceed 14 kHz to ensure that the lasing is close to saturation. Both sweep frequency limits, as specified by (4) and (5), could be increased through f_r, corresponding to shortening the cavity length. This could be achieved by cutting and splicing the fibre pigtails of the optical components inside the cavity. However, as the researched swept source is intended for a full field OCT system requiring sweep rates in the range of a few kHz, such a modification was not necessary for this study.

Experimentally, the polarisation state in the cavity is adjusted actuating on the PC in Fig. 1, affecting both the central lasing wavelength and the tuning range. The polarisation state was optimised to achieve the best compromise between the tuning range and the low amplitude ripple within the spectrum.

III. Results

The peak-hold spectra at the DTML-SS's output (without the BOA) using the pulse modulation for three different sweep rates f_s are displayed in Fig. 6 top graph. The faster the sweep rate, the larger the deterioration of the spectra, visible as the lower gain within the first half of the tuning range. This can be explained by the lower gain values below 850 nm of the used SOA, which may demand more round trips for the lasing wavelengths to reach saturation in comparison with the wavelengths in the right part of the spectrum. The deterioration for sweep rates larger than 15 kHz is evident, in line with the estimated value of 14 kHz obtained using (5). Fig. 5 displays the power at the DTML-SS's output against the sweep frequency.

By adding the BOA to the DTML-SS's output in Fig. 2, the output power increases to 8.2 mW at 10 kHz sweep rate, however, there is an ASE contribution from the BOA, visible in the spectra in Fig. 6 bottom graph. The reflective profiles (A-scans) roll-off measurements utilising the interferometer and the method of master-slave interferometry [20] are displayed in Fig. 7. First, a roll-off measurement for 25 nm tuning range using the sinusoidal modulation was performed. It can be seen that a short axial range of only $\Delta z = 0.3$ mm was was achieved. Then, the operating regime was switched to the pulse modulation, whose A-scans' sensitivity roll-offs against z for 35 nm tuning range are plotted in Fig. 7 as well. As it was predicted in the previous paragraph, despite keeping constant Δf_m in (2) for all examined sweep rates, the faster the sweeping, the lower the output power and poorer the axial resolution $\delta z \sim 1/\Delta\lambda$. The later is expected due to narrowing $\Delta\lambda$ values as shown in Fig. 6 bottom graph (measured as 6 dB drop in the PSD). The FWHM

axial resolution (measured on an A-scan peak close to zero axial coordinate z) for 10 kHz, 15 kHz and 20 kHz sweep rates are determined as 15 μm, 22 μm, and 44 μm, respectively. The measured value of 15 μm at 10 kHz sweep rate is close to the theoretical value $\delta z_{theory} = 0.60\lambda^2/\Delta\lambda \doteq 12\,\mu$m (for a top-hat spectrum shape [21]). However, no significant degradation in the axial range is observed, as for all three sweep rates similar values are obtained for a 50% drop in the amplitude corresponding to $\Delta z \doteq 1$ mm.

IV. Conclusion

In this letter, we demonstrated the combined use of a cFBG with a fast intensity modulator driven by short pulses to obtain more than 30 nm tuning range at shorter wavelengths such as 850 nm. In this way, better performance is obtained in comparison with a DTML-SS employing a SOA modulation [11]. The sweep frequency of 10 kHz could be further increased by shortening the cavity length, as indicated by (5). In addition, as presented in this study, coherence is significantly improved by applying short modulation windows of a 50 ps width. The linewidth is comparable to the linewidths reported in [1], [9], based on galvo filter and acousto-optic filter, respectively. We believe that by applying even shorter modulation windows, as allowed by technology of IM, the ASE could be further reduced and better coherence length achieved. This will also require advances in ultra short pulse generation. The swept source presented can find immediate applications in FFSS-OCT, replacing the current commercial sources available up to 2 kHz, and allowing even faster rates up to 10 kHz. Subject to further refinements, such as reducing its cavity length, even faster acquisition of volumes can be achieved to enable such a swept source to be paired with tens of kHz fast 2D CMOS cameras.

Disclosures

AP is an inventor and co-inventor of patents in the name of the University of Kent.

References

[1] M. F. Shirazi, P. Kim, M. Jeon, and J. Kim, "Full-field optical coherence tomography using galvo filter-based wavelength swept laser," *Sensors*, vol. 16, no. 11, pp. 1–9, 2016.

[2] J. Zhang et al., "Multi-MHz MEMS-VCSEL swept-source optical coherence tomography for endoscopic structural and angiographic imaging with miniaturized brushless motor probes," *Biomed. Opt. Exp.*, vol. 12, no. 4, pp. 2384–2403, Apr. 2021.

[3] R. Huber, M. Wojtkowski, and J. G. Fujimoto, "Fourier domain mode locking (FDML): A new laser operating regime and applications for optical coherence tomography," *Opt. Exp.*, vol. 14, no. 8, pp. 3225–3237, Apr. 2006.

[4] M. Bonesi et al., "Akinetic all-semiconductor programmable swept-source at 1550 nm and 1310 nm with centimeters coherence length," *Opt. Exp.*, vol. 22, no. 3, pp. 2632–2655, Feb. 2014.

[5] S. Grelet, A. M. Jiménez, R. D. Engelsholm, P. B. Montague, and A. Podoleanu, "40 MHz swept-source optical coherence tomography at 1060 nm using a time-stretch and supercontinuum spectral broadening dynamics," *IEEE Photon. J.*, vol. 14, no. 6, Dec. 2022, Art. no. 3963606.

[6] T. S. Kim et al., "9.4 MHz a-line rate optical coherence tomography at 1300 nm using a wavelength-swept laser based on stretched-pulse active mode-locking," *Sci. Rep.*, vol. 10, Jun. 2020, Art. no. 9328.

[7] J. Fujimoto and W. Drexler, *Opt. Coherence Tomography: Technol. Appl.*. Berlin, Germany: Springer, 2008.

[8] E. Auksorius et al., "In vivo imaging of the human cornea with high-speed and high-resolution Fourier-domain full-field optical coherence tomography," *Biomed. Opt. Exp.*, vol. 11, no. 5, pp. 2849–2865, May 2020. [Online]. Available: https://opg.optica.org/boe/abstract.cfm?URI=boe-11-5-2849

[9] G.-H. Han, S.-W. Cho, N. S. Park, and C.-S. Kim, "Electro-optic swept source based on AOTF for wavenumber-linear interferometric sensing and imaging," *Fibers*, vol. 4, no. 2, pp. 1–8, 2016.

[10] H. D. Lee, G. H. Kim, J. G. Shin, B. Lee, C.-S. Kim, and T. J. Eom, "Akinetic swept-source optical coherence tomography based on a pulse-modulated active mode locking fiber laser for human retinal imaging," *Sci. Rep.*, vol. 8, 2018, Art. no. 17660.

[11] S. Yamashita, N. Yuichi, K. Ryosei, and K. Osamu, "Wide and fast wavelength-swept fiber laser based on dispersion tuning for dynamic sensing," *J. Sensors*, vol. 2009, Jan. 2009, pp. 1–12.

[12] H. D. Lee, M. Y. Jeong, C.-S. Kim, J. G. Shin, B. H. Lee, and T. J. Eom, "Linearly wavenumber-swept active mode locking short-cavity fiber laser for in-vivo OCT imaging," *IEEE J. Sel. Topics Quantum Electron.*, vol. 20, no. 5, pp. 433–440, Sep./Oct. 2014.

[13] C. Zhang et al., "Low-cost dispersion-tuned active harmonic mode-locked laser with a 3-cm coherence length," *IEEE J. Sel. Topics Quantum Electron.*, vol. 20, no. 5, pp. 399–405, Sep./Oct. 2014.

[14] A. Takada, M. Fujino, and S. Nagano, "Dispersion dependence of linewidth in actively mode-locked ring lasers," *Opt. Exp.*, vol. 20, no. 4, pp. 4753–4762, Feb. 2012.

[15] H. Nagai and S. Yamashita, "Coherence improvement in dispersion-tuned swept laser by pulse modulation," *Electron. Lett.*, vol. 50, no. 23, pp. 1729–1731, 2014.

[16] R. Riha and A. Podoleanu, "An approximative fiber laser cavity dispersion assessment technique using mode-locked wavelength tuning," in *Opt. Coherence Tomography and Coherence Domain Opt. Methods in Biomed. XXVII*, Washington, DC, USA:Optica, 2022, p. 512.

[17] S. Yamashita and Y. W. Takubo, "Wide and fast wavelength-swept fiber lasers based on dispersion tuning and their application to optical coherence tomography," *Photonic Sens.*, vol. 3, pp. 320–331, 2013.

[18] Y. Hasegawa, T. Shirahata, and S. Yamashita, "Analysis of dynamic properties of dispersion-tuned swept lasers," *J. Lightw. Technol.*, vol. 33, no. 1, pp. 219–226, Jan. 2015.

[19] R. Huber, M. Wojtkowski, K. Taira, J. G. Fujimoto, and K. Hsu, "Amplified, frequency swept lasers for frequency domain reflectometry and OCT imaging: Design and scaling principles," *Opt. Exp.*, vol. 13, no. 9, pp. 3513–3528, May 2005. [Online]. Available: http://www.opticsexpress.org/abstract.cfm?URI=oe-13-9-3513

[20] A. G. Podoleanu and A. Bradu, "Master–slave interferometry for parallel spectral domain interferometry sensing and versatile 3D optical coherence tomography," *Opt. Exp.*, vol. 21, no. 16, pp. 19324–19338, 2013.

[21] J. P. Fingler, "Motion contrast using optical coherence tomography," Ph.D. dissertation, Dept. Eng. Appl. Sci., California Inst. Technol., Pasadena, CA, USA, Jul. 2007.